AGU PUBLICATIONS

JGR

Journal of Geophysical Research: Atmospheres

RESEARCH ARTICLE
10.1002/2017JD027316

Key Points:
- ToF-CIMS identifies isocyanates, amides, nitro-organics, and nitrates with mixing ratio enhancements between 2 and 13 times during bonfire night
- Low wind speeds and poor mixing favor pollutant accumulation with HNCO concentrations reaching potentially harmful levels
- While this event is highly polluting, NO_2 concentrations at this site are higher at other times most likely due to emissions from traffic

Supporting Information:
- Supporting Information S1

Correspondence to:
C. J. Percival,
carl.j.percival@jpl.nasa.gov

Citation:
Priestley, M., Le Breton, M., Bannan, T. J., Leather, K. E., Bacak, A., Reyes-Villegas, E., et al. (2018). Observations of isocyanate, amide, nitrate, and nitro compounds from an anthropogenic biomass burning event using a ToF-CIMS. *Journal of Geophysical Research: Atmospheres*, *123*. https://doi.org/10.1002/2017JD027316

Received 30 JUN 2017
Accepted 14 FEB 2018
Accepted article online 27 FEB 2018

Observations of Isocyanate, Amide, Nitrate, and Nitro Compounds From an Anthropogenic Biomass Burning Event Using a ToF-CIMS

Michael Priestley[1], Michael Le Breton[1,2], Thomas J. Bannan[1], Kimberly E. Leather[1], Asan Bacak[1], Ernesto Reyes-Villegas[1], Frank De Vocht[3], Beth M. A. Shallcross[4], Toby Brazier[5], M. Anwar Khan[5], James Allan[1,6], Dudley E. Shallcross[5], Hugh Coe[1], and Carl J. Percival[1,7]

[1]Centre for Atmospheric Science, School of Earth and Environmental Sciences, University of Manchester, Manchester, UK, [2]Now at Department of Chemistry and Molecular Biology, University of Gothenburg, Göteborg, Sweden, [3]School of Social and Community Medicine, University of Bristol, Bristol, UK, [4]Division of Pharmacy and Optometry, University of Manchester, Manchester, UK, [5]School of Chemistry, University of Bristol, Bristol, UK, [6]National Centre for Atmospheric Science, University of Manchester, Manchester, UK, [7]Now at Jet Propulsion Laboratory, Pasadena, CA, USA

Abstract Anthropogenic biomass burning is poorly represented in models due to a lack of observational data but represents a significant source of short-lived toxic gases. Guy Fawkes Night (bonfire night) is a regular UK-wide event where open fires are lit and fireworks are set off on 5 November. Previous gas phase studies of bonfire night focus on persistent organic pollutants primarily using off-line techniques. Here the first simultaneous online gas phase measurements of several classes of compounds including isocyanates, amides, nitrates, and nitro-organics are made during bonfire night (2014) in Manchester, UK, using a time-of-flight chemical ionization mass spectrometer (ToF-CIMS) using iodide reagent ions. A shallow boundary layer and low wind speeds favor pollutant buildup with typical HCN, HNCO, and CH_3NCO concentrations of tens of parts per thousand increasing by a factor of 13 to potentially harmful levels >1 ppb. Normalized excess mixing ratios relative to CO for a range of isocyanates and amides are reported for the first time. Using a HNCO:CO ratio of 0.1%, we distinguish emissions from flaming and smoldering combustion and report more accurate normalized excess mixing ratios for the distinct burning phases. While bonfire night is a highly polluting event, NO_2 concentrations measured at this location are higher at other times, highlighting the importance of traffic as an NO_2 emission source at this location. A risk communication methodology is used to equate enhancements in hourly averaged black carbon and NO_2 concentrations caused by bonfire night as an equivalent of 26.1 passively smoked cigarettes.

1. Introduction

Biomass burning (BB) is a major source of gas and carbonaceous aerosol emission to the atmosphere (Andreae & Merlet, 2001), both of which act to reduce air quality worldwide (Molina et al., 2007). Solid biofuel burning makes up part of the anthropogenic contribution to BB, being the primary source of heating and cooking for 3 billion people worldwide (World Health Organization, 2015). Emissions from BB affect large population centers across the globe. For example, in New Delhi, India, a mega city with a population of 26,454,000 (United Nations, 2016), approximately 99% of inhabitants are exposed to more $PM_{2.5}$ than the 10 $\mu g\ m^{-3}$ WHO air quality guideline (World Health Organization, 2006). An estimated 20% of the $PM_{2.5}$, which contributes to this exposure originates from open BB (Amann et al., 2017). While this is not necessarily as important in the UK, solid biofuel burning is becoming more popular for financial, esthetic, and environmental reasons (Caird et al., 2008) and is significant in its contribution to reducing air quality (Fuller et al., 2014). One example of a regular, nationwide BB event in the UK is Guy Fawkes Night, or bonfire night, which is celebrated annually on and around 5 November by lighting open fires and fireworks as part of community events and at individual households. These bonfires are lit at roughly the same time during the evening and are designed to have a strong flaming phase that lasts for 1–2 h. After flaming, the fires are not refueled and so there is an extended period of smoldering as the fires are left to die away. The UK Environment Agency permits the open burning of untreated wood and garden waste (UK Government 2015) and states that treated materials and household waste (solvents, plastics, etc.) should not be burnt, although it is likely that these types of materials do contribute to the composition of bonfire night open fires. This mixed fuel source is difficult to categorize and most likely represents a mixture of residential biofuel combustion and garbage

burning, the latter of which is poorly characterized across the globe and known to emit many toxic compounds (Akagi et al., 2011, and references therein).

It is known that bonfire night is among the most polluted days in terms of air quality in the UK (Dyke et al., 1997; Mari et al., 2010; Pongpiachan et al., 2015). Bonfire night exhibits significantly elevated particle levels compared with the year average at all urban sites in the UK (Harrison & Shallcross, 2011), and inspection of long-term measurement sites such as the Marylebone Road site in London shows that the night associated with bonfire night (it may be the Friday, Saturday, or Sunday closest to 5 November) would appear to be the highest in terms of pollution with associated implications for human health. The effects of open fire and firework events on enhancing metalliferous particles (Moreno et al., 2007), aerosol (Vassura et al., 2014), and trace gas concentrations (Drewnick et al., 2006) including volatile organic compounds (VOCs) are well documented. Much of the data on gaseous pollutants collected during previous bonfire nights in the UK have focused on persistent organic pollutants (Farrar et al., 2004; Harrad & Laurie, 2005), which have been linked to climate change (Nadal et al., 2015) and are linked to adverse human health effects including cancer (Mouly & Toms, 2016) and reproductive diseases (Bonde et al., 2016). Sampling of specific pollutants has mainly been off-line, using whole air sampling or filter collection, reducing the temporal resolution of the data sets. Advances in measurement techniques such as the development of the time-of-flight chemical ionization mass spectrometer (ToF-CIMS) (Bertram et al., 2009) with its high selectivity, sensitivity, resolution, and data acquisition rate permit enhanced detectability of short-lived, toxic, nonpersistent organic pollutants trace gases in real time.

Hydrogen cyanide (HCN) is one such highly toxic gas and known BB tracer (e.g., Yokelson et al., 2007) with a typical lifetime of 2–4 months (Li et al., 2009) that has previously been measured by iodide CIMS (e.g., Le Breton et al., 2013). Globally, the greatest sources of HCN to the atmosphere are biogenic, via cyanogenesis, and BB (Li et al., 2003; Shim et al., 2007), which is known to be highly variable and strongly dependent on fuel type (Akagi et al., 2011; Coggon et al., 2016). In urban locations, a significant contribution to ambient HCN originates from vehicles (Moussa et al., 2016).

Isocyanic acid (HNCO) is another highly toxic, long-lived gas (lifetime of days to decades; Borduas et al., 2016) emitted from BB with similar anthropogenic and biogenic sources as HCN. Urban sources of HNCO are attributed to primary activity such as automotive emission (Jathar et al., 2017), residential heating (BB) (Woodward-Massey et al., 2014), and industrial processes, for example, from brick kiln emissions (Sarkar et al., 2016). A secondary source of HNCO is amide oxidation (e.g., Borduas et al., 2015), which has been observed at a suburban site in Mohali, India (Chandra & Sinha, 2016), and in an urban environment in Pasadena, California (Roberts et al., 2014). Mean urban concentrations of HNCO are variable having previously been measured to be on the order of 10–100 ppt by acetate CIMS in Pasadena (Roberts et al., 2014) and ~1 ppb using a proton transfer reaction-mass spectrometer (MS) in Mohali (Chandra & Sinha, 2016). This higher level is attributed to a strong regional background potentially caused by the oxidation of another set of precursors, alkyl amines, originating from agricultural BB (Sarkar et al., 2016, 2017). In addition to its toxicological importance, HNCO measurements are useful as the criteria of [HNCO]/[CO] has been used to define the separation of flaming from smoldering combustion phases (Roberts et al., 2011). Methyl isocyanate (MIC) is a homologue of HNCO and a known secondary pollutant with precursors originating from both biogenic and anthropogenic sources (Lu et al., 2014; Woodrow et al., 2014) MIC has been measured as a direct emission from industrial processes and the burning of common building materials (Blomqvist et al., 2003; Henriks-Eckerman et al., 2002).

Amides are known products of BB (e.g., Stockwell et al., 2015) and from the burning of household materials (Kim et al., 2015). These compounds are known toxins (Gescher, 1990), which, as previously mentioned, are also precursors to isocyanic compounds (Borduas et al., 2015). In Shanghai, Yao et al. (2016) found that amides with greater than three carbon atoms were prevalent over lower mass amides, with concentrations on the order of parts per billion (ppbs) suggesting both secondary and industrial primary sources.

Organic nitrates are another class of toxic compounds with wide implications for atmospheric chemistry. They are a reservoir of NO_2, thus enabling the transport of NO_x and subsequent ozone formation at remote locations, and are typically semivolatile, contributing to secondary organic aerosol formation and thus particulate matter (PM) with further associated air quality issues. Other nitrates such as peroxynitric acid have previously been detected by iodide CIMS (Veres et al., 2015) and peroxyacetyl nitrate (PAN), which has previously

been detected by PAN iodide CIMS (Veres & Roberts, 2015). Nitro-organic compounds such as nitrophenol and its degradation products, which have been shown to be genotoxic (Sekler et al., 2004), have many sources including vehicular emission, degradation of pesticides (Lüttke et al., 1997, and references therein), secondary gas phase reactions (Berndt & Böge, 2006), and aqueous aerosol phase reactions (Yuan et al., 2015) and have vapor pressures low enough to readily partition into the condensed phase (Bannan et al., 2017). Nitrophenols, methyl nitrophenols, and nitrocatechols have been detected in laboratory BB smoke using ToF-MS (Iinuma et al., 2010) and also in urban plumes (Mohr et al., 2013).

Measurements were carried out from 29 October 2014 to 11 November 2014 at the University of Manchester to assess the impact of bonfire night activity on local air quality and to probe the complex composition of an urban BB plume using novel identification methods to identify toxic species that currently do not feature in air quality health assessments.

2. Methodology

2.1. Site Description

Manchester is located in the center of Greater Manchester Metropolitan County, an administrative area encompassing 10 different metropolitan boroughs of mostly urban districts, with a collective area of 1,276 km^3 and a population of 2.6 million inhabitants. The Whitworth Observatory is an urban rooftop measurement site approximately 15 m above street level and 100 m from the nearest road, located in the Simon Building at the University of Manchester's south campus, approximately 1.5 km south of Manchester City Centre (53.467°N, 2.232°W). For a map of the measurement location and sites of large-scale public bonfires, see Reyes-Villegas et al. (2017).

2.2. Instrument Description

2.2.1. Time-of-Flight Chemical Ionization Mass Spectrometer

A high-resolution ToF-CIMS as described by Lee et al. (2014) was deployed to measure a vast suite of atmospheric species using the iodide reagent ion. It consists of a reduced pressure ion molecule reaction (IMR) region coupled to a Tofwerk atmospheric pressure interface high-resolution time-of-flight mass spectrometer (Junninen et al., 2010). The instrument has been described in detail elsewhere (Lee et al., 2014); here we describe the specific details related to its setup for this campaign.

The IMR was held at a constant pressure of 100 mbar by a scroll pump (Agilent SH-112) controlled with a servo control valve placed between the scroll pump and IMR. Ambient air was drawn into the IMR via a critical orifice at 2.2 standard liters per minute (slm). The reagent I^- ions were created by flowing 10 standard cubic centimeters per minute of methyl iodide (CH_3I) emitted from a permeation tube held at 40°C through 1/8″ perfluoro alkoxy (PFA), which is carried by a 2 slm nitrogen (N_2) flow through a Po-210, 10 mCi, alpha emitting reactive ion source (NRD Inc Static Solutions Limited) orthogonal to the ambient flow into the IMR. Once in the IMR, the I^- ions then ionize species of interest. The ionizer and ambient air flows mixed for approximately 30 ms until a fraction of the flow was sampled through an orifice into the first of four differentially pumped chambers in the ToF-CIMS. The first chamber was held at 150 mbar by a scroll pump (Triscroll 600), and the second stage was pumped by a split flow turbo molecular drag pump and held at 1.50 mbar. Quadrupole ion guides transmit the ions through these stages while simultaneously providing extracollisional cooling and energetic homogenization of the ions as they enter the extractor region. The electric field strengths in the axial direction (<2 V/cm) were set to optimize the total ion signal and transmission of the iodized species of interest (E/N ratio of 65 Td). Optimization of the $I{\cdot}H_2O^-$ cluster signal is considered essential to optimize system sensitivity since the detection of particular compounds, for example, formic acid, is dependent on the number of $I{\cdot}H_2O^-$ adducts. The ions were subsequently pulsed into the drift region of the ToF-CIMS at 22.22 kHz where the arrival time is detected with a pair of microchannel plate detectors. The mass calibration was performed for seven known masses: NO_3^-, I^-, $I^-{\cdot}H_2O$, $I^-{\cdot}HCOOH$, $I^-{\cdot}HNO_3$, I_2^-, and I_3^-, which covers a range of 62 to 381 *m/z*. The mass calibration was fitted to a third-order polynomial and was accurate to within 2 ppm; ensuring that peak identification was accurate below 20 ppm. The resolution was 3,560 at 127 *m/z* and 3,845 at 381 *m/z*. All species reported are observed as adducts with I^-.

2.2.1.1. Sampling, Calibration, and Backgrounds

To minimize sampling losses through the inlet tubing, a fast inlet pump is implemented to sample at 15 slm through 1 m long ¾″ PFA tubing. This translates to an inlet residence time of 1.2 s. Approximately 2.2 slm of

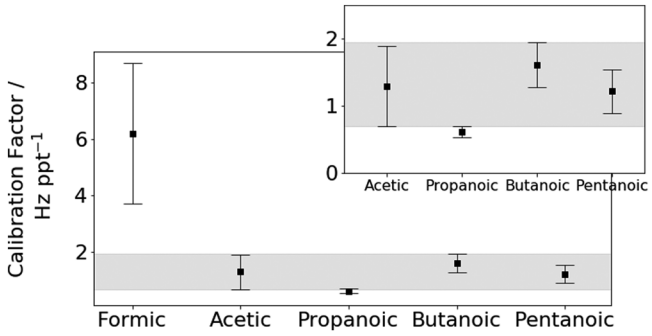

Figure 1. Time-of-flight chemical ionization mass spectrometer C_1–C_5 organic acid calibration factors. (inset) C_2–C_5 calibration factors show similar sensitivities. Error bars represent ±2σ. The gray area represents upper and lower errors of C_2–C_5 calibration factors.

the centerline flow is subsampled into the IMR of the ToF-CIMS through a conical shaped critical orifice, while the remaining flow is exhausted by the scroll pump. Backgrounds were taken every 6 h for 20 min by overflowing the inlet to the IMR with dry N_2.

As the ToF-CIMS is able to detect 10^2–10^3 species, calibration becomes difficult. One methodology to simplify calibration is to apply a uniform calibration factor using a maximum sensitivity based on adduct formation at the collision limit and assuming maximum transmission efficiency (Ehn et al., 2014; Lopez-Hilfiker et al., 2015). Another methodology makes use of an average organic acid calibration factor (Chhabra et al., 2015), while others aim to derive sensitivities from binding enthalpies of the reagent ion (Iyer et al., 2016). Here we apply the laboratory-determined calibration factors for a series of C_1 to C_5 aliphatic organic acids to species with an equivalent number of carbon atoms, assuming that the carbon number dictates the collision limit of adduct formation.

Above a carbon number of 2 within this particular series, the calibration factor is independent of *m/z* (Figure 1). We use this assumption to apply a uniform calibration factor of 6.20 Hz ppt^{-1}, derived from formic acid, for C_1 compounds and a calibration factor of 1.28 Hz ppt^{-1}, derived from acetic acid, for C_n compounds ($n > 1$).

Formic acid was both measured and calibrated for throughout the campaign by adding known concentrations of HCOOH as previously described in Le Breton et al. (2012). The ToF-CIMS HCN signal was cross calibrated with the calibrated quad-CIMS. Known concentrations of HCN were produced by flowing from a HCN calibration cylinder (BW Technologies) that was diluted from 10 ppm mix with an accuracy of ±10% as described by Le Breton et al. (2013) (supporting information S1). The sensitivity of the quad-CIMS to HNCO is assumed to be the same as HCN. The sensitivity of the quad-CIMS and ToF-CIMS is shown in Table 1.

Sensitivity changes due to reagent ions are minimal. Mean average I^- + $I{\cdot}H_2O^-$ counts were high ($3.52 \times 10^6 \pm 5.2 \times 10^5$ (1σ)) and well above the threshold where we observe a much reduced dependency of sensitivity on reagent ion count (Le Breton et al., 2014). We normalize to I^-, $I{\cdot}H_2O^-$, or the sum of both depending on which has the best correlation with the signal of the species of interest. If there is no discernable correlation, no normalization takes place. None of the signals for the species reported in this manuscript were normalized to $I{\cdot}H_2O^-$ or the sum of I^- + $I{\cdot}H_2O^-$.

The calibration standard stock solutions for each acid were made with 95–97% reagent grade organic acids (Sigma-Aldrich) to produce 1% volume per volume solutions in water. These stock solutions were subsampled to make calibration standards ranging from 0.1 to 1.1 ppm. About 100 μL of calibration standard was injected into an evacuated Pyrex impinger connected to the evacuated 118 L Extreme Range Reaction Chamber (Leatheret al., 2010). The calibration standard volatilizes when exposed to the evacuated system, and partitioning to the gas phase is aided by passing N_2 carrier gas through the impinger until the chamber is filled to ~760 torr (1.74% error). Calibration mixes of 500, 1,000, and 2,000 ppt are subsampled by the ToF-CIMS through 70 cm ¼" PFA tubing. Blank water backgrounds were performed before every calibration by injecting 100 μL of water and the lines cleaned with N_2 between sampling. These calibrations were performed postcampaign and compared with in-house made gas mixtures as described in Bannan et al. (2015) showing the same results to within 5% error.

A literature survey (Brophy & Farmer, 2015; Iyer et al., 2016; Lee et al., 2014; Veres & Roberts, 2015) of formic acid calibration factors (normalized to 1 × 10^6 Hz reagent ion) provides a range between 2.9 and 13 Hz ppt^{-1} (with reported errors of 0.6–5.0 Hz ppt^{-1}) highlighting

Table 1
Calibration Factors for the ToF-CIMS Used in This Study

	Calibration factor (Hz ppt^{-1})		
Compound	Quad-CIMS	ToF-CIMS	ToF-CIMS 2σ error
HCN	4	1.93	-
HNCO	4	2.65	-
Formic acid (C_1)	-	6.20	2.48
Acetic acid (>C_1)	-	1.28	0.60
Propanoic acid	-	0.61	0.08
Butanoic acid	-	1.61	0.33
Pentanoic acid	-	1.21	0.33

Note. ToF-CIMS = time-of-flight chemical ionization mass spectrometer.

Table 2
Measurements, Resolutions, and Accuracies of Meteorological Instruments at the Whitworth Observatory

Parameter	Instrument	Resolution	Accuracy
Wind speed	Gill Windmaster Pro Sonic Anemometer	0.01 ms^{-1}	1.50%
Wind direction	Gill Windmaster Pro Sonic Anemometer	0.10°	2.00%
Temperature	Rotronics MP100-H mounted in Rotronics Aspirated Radiation Shield (RS12T)	0.10°C	0.30°C
Relative humidity	Rotronics Hygroclip	0.10%	1.50%
Barometric pressure	Vaisala PTB10 Digital Barometer with Vaisala SPH10 Static Pressure Head	0.01 hPa	0.30 hPa
Direct solar radiation	Kipp and Zonen CMP-11 Pyranometer	—	2.00%
NO_x ($NO + NO_2$)	Thermo Scientific 42i	0.40 ppb	0.40 ppb
O_3	Casella ML2010	10.00 ppb	10.00 ppb
CO	Thermo Scientific 48i	0.10 ppm	0.04 ppm
SO_2	Thermo Scientific 43i-TLE	0.20 ppb	0.05 ppb

the variation in sensitivity that is associated with the instruments' condition and circumstance for this particular compound. Our formic acid calibration factor of 6.20 ± 1.28 Hz ppt^{-1} (4.13 ± 0.85 Hz ppt^{-1} normalized to 1×10^6 Hz reagent ion) is well within this range. Of 61 compounds surveyed in the literature, a range of calibration factors from 7.6×10^{-5} to 22 Hz ppt^{-1} with a mean sensitivity and error of 5.20 ± 0.97 Hz ppt^{-1} and 1σ = 6.61 Hz ppt^{-1} further demonstrate the variability of the detection capabilities of the ToF-CIMS.

2.2.2. Meteorology and Air Quality

Meteorological measurements (pressure, temperature, relative humidity, wind speed and direction, precipitation, visibility, and actinic flux) are made approximately 100 m away on the nearby George Kenyon Building approximately 40 m above ground level in the University's south campus (approximately 53.466°N, 2.232°W). For a map of the measurement site and large-scale public bonfires, see Reyes-Villegas et al. (2017). Temperature, humidity, pressure, and wind speed and direction instruments are located approximately 3–5 m above the surface of the station to reduce the impact of the building below on the measurements being made. A summary of meteorological measurements, instruments, ranges, resolutions, accuracies, and data collection frequencies is summarized in Table 2. Automated high-frequency (0.1 Hz) long-term trace gas measurements of NO_x, O_3, CO, and SO_2 are made at the same location as the ToF-CIMS measurements. It is noted that the NO_x measurement technique uses a molybdenum catalyst that is known to cause an overestimation of NO_2 concentrations by the nonselective conversion of NO_y species as well as NO_2 to NO, which is actively detected by chemiluminescence. However, as the UK automatic urban rural network also uses this technique to measure NO_x, the results presented here should be comparable. A lack of CO_2 measurements prevents the calculation of modified combustion efficiencies (MCEs) (Yokelson, Griffith, & Ward, 1996).

2.3. Kendrick Mass Defect

Kendrick mass defect (KMD) analysis is a mass spectrometric data analysis technique used to identify individual species in complex mixtures. While KMD analysis has been used to study the chemical composition of secondary organic aerosol (SOA) (Walser et al., 2008), it relies on a high-resolution ($m/\Delta m > 50{,}000$) typical of magnetic sector instruments with high accuracies, for example, <1 ppm (Bristow & Webb, 2003).

The average resolution of the ToF-CIMS was 3,800, and accuracy was <20 ppm. While these metrics indicate that the instrument is not able to unequivocally distinguish individual species, it is possible to use KMD analysis to suggest potential chemical formulae for unknown species if we account for the error in exact mass peak assignment and the selectivity of the I^- reagent ion.

From the ToF-CIMS high-resolution mass spectra recorded over the campaign, a total of 652 peaks was manually identified; 75 peaks were first identified by a priori knowledge and by using peak fitting software, leaving 577 unknown assignments.

The peak list, containing the 75 known assignments, was then run through a program that matches known and unknown species that share the same KMD (within error) when normalized to different moieties (e.g., CH_2, O, and CHO) as well as ^{12}C. The procedure is as follows: Where the *m/z* of the unknown assignment is

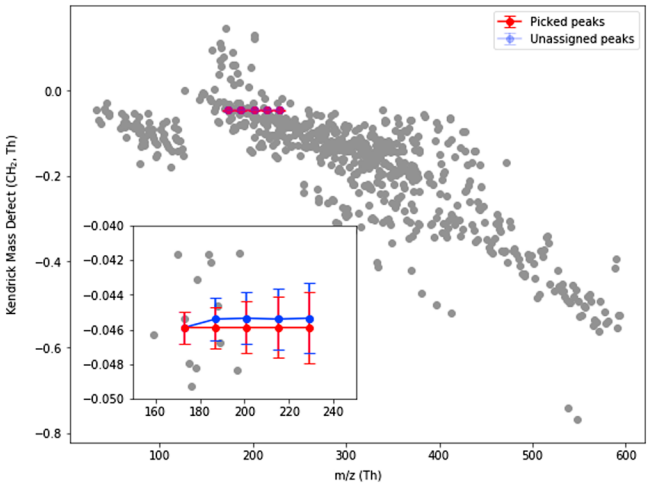

Figure 2. Kendrick mass defect plot of the identified peaks in this data set (gray). (inset) Exact masses (red) and measured masses (blue) of the C_1–C_5 organic acids in CH_2 Kendrick mass defect space. Error bars show propagated 20 ppm error. All measured peaks are well within error. The exact masses (red) show where the measured masses should be found on this plot, connected by a straight line. Where the assignment is measured (picked, blue), the error in the exact mass is visible as a deviation from the straight line. The transition from formic to acetic acid shows a deviation in the straight line, which is a manifestation of the systematic error in the mass axis. All subsequent measured peaks sit on a straight line, indicating that there is no more deviation, and so the error in the mass axis is propagated but not compounded.

an integer *n* times the *m/z* of the known assignment, it is interpreted that the assignments are related in KMD space and the formula of the unknown assignment can be determined from the known assignment (±*n* moieties). These potential assignments are assessed for their validity in terms of realistic structures and detectability by the ionization method. Figure 2 shows the total number of peak assignments as well as the known assignment of formic acid and the ability of the program to identify four "unknowns" in the same series, that is, the C_2-C_5 organic acids.

As this technique relies heavily on high mass accuracy, accurate mass calibration and peak shape are vitally important. Peak assignments are treated as indicative and cannot account for isomeric or isobaric compounds. A sample of the chemical formula and suggested chemical species identified by this technique in conjunction with time series correlation analysis is discussed below, and isocyanate, nitrate, nitro, and amide compounds are tentatively assigned.

3. Results and Discussion

3.1. Pollution Events

Diurnal profiles of CO and NO_x concentrations show a prominent daily bimodal cycle associated with traffic rush hours (07:00–10:00 UTC and 16:30–18:00 UTC). At the peak of the morning rush hour (approximately 08:30) average CO and NO_x concentrations peak at 225 ppb and 31 ppb and again at 250 ppb and 30 ppb during the evening rush hour at 16:45. Minima for both species are observed during the early morning (04:35), with average values of 146 ppb and 5 ppb. Periodic stagnation events occur when wind speeds are low ($<$2.0 ms^{-1}) with the highest concentrations of NO_x and CO measured when these events coincide with a rush hour period. At these times, CO and NO_x concentrations reach, at their maximum, 400 ppb and 508 ppb, respectively. Figure 3 summarizes the measurement period. All measurements are reported as 1 min averages.

3.2. Bonfire Night

Bonfire night (5 November) is defined as the period between 16:30 on 5 November and 07:30 on 6 November. During this period, the mean pressure was 998 hPa, mean temperature was 5.4°C (lowest during the campaign), and mean wind speed was 1.89 m s^{-1}. This combination of high pressure, low temperature, and low wind speed is indicative of a stable, shallow boundary layer and poor dispersion, increasing the buildup of pollutants. No one bonfire was directly sampled; instead, a mixture from multiple sources (both private and public) was accumulated and mixed together forming a homogenous air mass dominating the conventional background. NO_x measurements from the UK automatic urban rural network monitoring network (Manchester Piccadilly, Manchester South, Salford Eccles, Glazebury) recorded maxima with varying wind directions and show little correlation with nearby large-scale events further suggesting that over a wider geographical area, the air mass composition cannot be attributed to any one single event (S2).

3.2.1. Identifying the Bonfire Burn Period Using BB Markers

CIMS has previously been used to identify BB plumes using a statistical approach (Le Breton et al., 2013) where the concentration of a BB marker (e.g., HCN) above 6 times the standard deviation of its median background concentration is used to define a BB plume. As previously stated, no one plume during bonfire night could be identified individually. However, as bonfire night burning broadly follows a regimented schedule of prescribed activity (with flaming phase combustion occurring for 1–2 h during the early evening and smoldering thereafter lasting well into the next morning), this approach to defining in-plume sampling is applicable in identifying the temporal bounds of bonfire night burning activity, from here termed the bonfire burn period (BBP). HCN and isocyanic acid (HNCO) were used as BB markers to which the 6 sigma methodology was applied. The BBP started at approximately 16:00 and ended between 04:00 and 05:00. As HCN is more

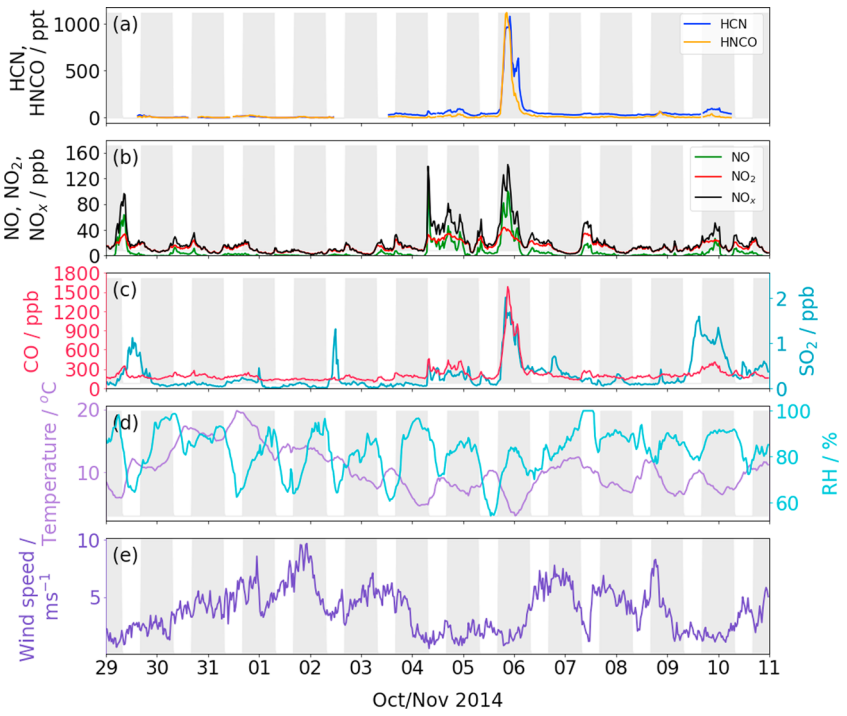

Figure 3. Time series of key measurements during the campaign (30 min averaged). (a) HCN and HNCO; (b) NO, NO_2, and NO_x; (c) CO and SO_2; (d) temperature and relative humidity; and (e) wind speed. Nongray background indicates daylight (approximately 07:30–16:30).

Table 3
Top 20 Correlations of HCN and HNCO With Other Measured Species During the BBP

	HNCO			HCN		
	Formula	Identified as	R^2	Formula	Identified as	R^2
1	$C_4H_6O_6$	Tartaric acid	0.95	HONO	Nitrous acid	0.97
2	$C_3H_4O_2$	Acrylic acid	0.95	NO_x	NO_x	0.94
3	$C_4H_6O_2$	Butanoic acid	0.94	C_2H_5NO	*N*-Methylformamide	0.94
4	$C_3H_3NO_3$	2,4-Oxazolidinedione	0.94	$C_2H_7NO_3$	—	0.94
5	HCN	Hydrogen cyanide	0.93	$C_4H_6O_2$	Butanoic acid	0.93
6	$C_2H_3NO_2$	*N*-Formylformamide	0.93	$C_2H_5N_3O_3$	—	0.93
7	HONO	Nitrous acid	0.92	HNCO	Isocyanic acid	0.93
8	CH_3NCO	Methyl isocyanate	0.92	NO_2	Nitrogen dioxide	0.93
9	CH_4O_2	Methanediol	0.91	NO	Nitric oxide	0.93
10	CH_2O_2	Formic acid	0.91	$C_7H_{14}O_6$	—	0.92
11	$C_7H_{14}O_6$	—	0.90	C_3H_7NO	*N*,*N*-Dimethylformamide	0.92
12	NO_2	Nitrogen dioxide	0.90	C_3H_7NO	Acrylamide	0.92
13	$C_5H_6O_2$	—	0.89	$C_5H_6O_2$	—	0.91
14	C_3H_7NO	Acrylamide	0.89	$C_4H_6O_6$	Tartaric acid	0.91
15	C_2H_5NO	*N*-Methylformamide	0.88	C_6H_6O	Phenol	0.91
16	C_6H_6O	Phenol	0.88	$C_2H_3NO_2$	*N*-Formylformamide	0.90
17	NO_x	NO_x	0.88	$C_3H_4O_2$	Acrylic acid	0.90
18	$C_2H_7NO_3$	—	0.87	$C_7H_6O_2$	Benzoic acid	0.90
19	$C_5H_4O_4$	—	0.86	$C_5H_4O_4$	—	0.90
20	$C_3H_6O_2$	Propanoic acid	0.86	$C_5H_8O_4$	Glutaric acid	0.87

Note. BBP = bonfire burn period.

Table 4
Mean and Maximum Concentrations of Selected Species With Bonfire Plume Removed, Maximum Concentration Measured During the BBP Only, and Limit of Detections

Formula	Mass (Da)	Identified as	Compound	BBP removed		BBP only	LOD (ppt)
				C_{mean} (ppt)	C_{max} (ppt)	C_{max} (ppt)	
HCN	154	Hydrogen cyanide		35	132	1,235	2.59
HNCO	170	Isocyanic acid	Isocyanate	12	144	1,639	2.70
CH_3NCO	184	Methyl isocyanates	Isocyanate	61	327	4,299	14.00
$C_3H_3NO_2$	212	Cyano acetic acid	Isocyanate	10	65	84	1.41
CH_3NO_4	220	Nitroperoxy methane	Nitrate	8	20	31	2.86
$C_2H_3NO_5$	248	PAN	Nitrate	54	221	15	4.90
$C_6H_5NO_3$	266	Nitrophenol	Nitro	131	530	630	15.62
$C_7H_7NO_3$	280	Methyl nitrophenol	Nitro	96	299	550	7.28
$C_6H_9N_3O_6$	346	Trinitrocyclohexane	Nitro	14	133	73	2.82
CH_3NO	170	Formamide	Amide	10	25	189	2.05
C_2H_5NO	186	*N*-Methylformamide	Amide	9	23	275	3.75
C_3H_5NO	198	Acrylamide	Amide	15	52	148	2.43
$C_2H_3NO_2$	200	*N*-Formylformamide	Amide	26	95	100	3.30
C_3H_7NO	200	*N*,*N*-Dimethylformamide	Amide	8	16	102	3.72

Note. BBP = bonfire burn period; LOD = limit of detections.

routinely measured, with elevated concentrations suggested unique to BB, it is chosen preferentially to define the BBP.

Within the BBP, HCN and HNCO correlate with 184 and 140 species where 82 common species have $R^2 > 0.75$. The correlated species are detected at elevated concentrations at an early stage during the evolution of the BBP. A summary of the 20 identified species with the strongest correlations with HCN and HNCO is shown in Table 3.

Table 4 summarizes mean and maximum concentrations of nitrogen-containing compounds during the measurement period and the maximum concentration during the BBP. The limit of detection (LOD) reported is 3 times the standard deviation of the background measured at 1 min time resolution. Generally, concentrations of all species are highest during the BBP than at any other point. Two exceptions are PAN and trinitrocylcohexane. LODs range from one to tens of ppt.

Not including the BBP, 19 ± 13% (1σ) of the 0.32 μg m^{-3} mean total detected mass (including all unknown peaks) can be attributed to the 75 identified peaks. This percentage is conserved at the highest mass loading (1.00 μg m^{-3}) recorded for this period. However, during the BBP the fraction of identified material increases to 24 ± 21%, and the mean total detected mass increases to 0.70 μg m^{-3}. At the highest mass loading of 2.0 μg m^{-3} during the BBP, the fraction of identified material further increases to 41%. The five largest organic concentration enhancements between the BBP and non-BBP are identified as $C_6H_6O_2$, $C_6H_6O_3$, CH_2O_2, $C_3H_6O_3$, and $C_7H_8O_2$.

3.2.2. Identification and Behavior of Key Species

Excluding the BBP, the mean ambient HCN concentration of 35 ppt and maximum concentration of 132 ppt is comparable with other ground-based HCN measurements, both rural and urban (Ambrose et al., 2012; Knighton et al., 2009). The species with the highest correlations with HCN with the BBP removed are propanoic acid (R^2 = 0.79), HONO (R^2 = 0.76), MIC (R^2 = 0.75), formamide (R^2 = 0.71), and *N*-methylformamide (R^2 = 0.68). Figure 4 summarizes diurnal profiles of selected species with the bonfire night period overlaid.

Low HCN concentrations <10 ppt were more commonly measured during weekends and during the nighttime when anthropogenic activity is at a minimum. Low concentrations were also measured when wind speeds were high and the wind direction was southwesterly, associated with cleaner, inflowing air masses.

Typical HCN concentrations of 30–50 ppt were most commonly observed during weekdays, when wind speeds were greater than 3.0 ms^{-1} (with no dependence on wind direction). Combined with a diurnal

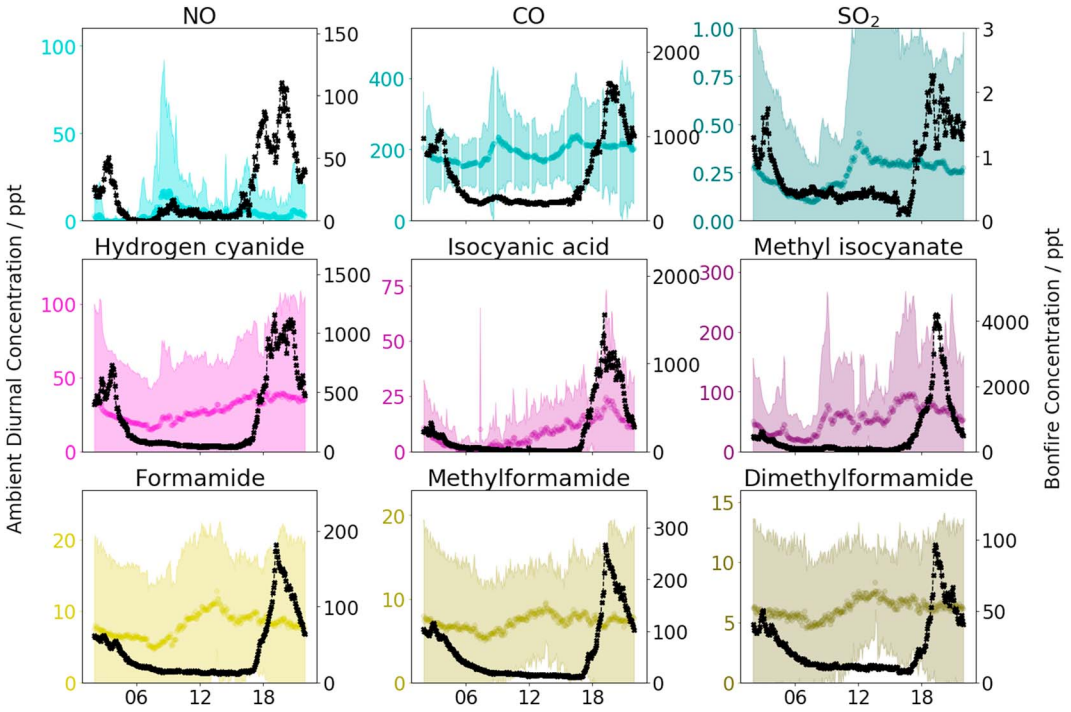

Figure 4. Five minute averaged ambient diurnal profiles of identified species throughout the campaign with the bonfire burn period removed (colored, left axis) and the shaded area representing 95% variation. Right axis and black trace show concentration and profile of the bonfire burn period starting at 16:30 on 5 November (nightfall) and extending to 16:30 on 6 November demonstrating the elevation and nontypical behavior of these compounds.

profile that does not exhibit a local emission signal (Figure 4), this range of concentrations is suggestive of a regional rather than local signal.

For the weekdays of 30 October and 4, 5, and 7 November between the hours of 07:00 and 09:00, HCN concentrations >50 ppt and a positive linear relationship with NO (R^2 = 0.67, 0.94, 0.73, and 0.59, respectively) demonstrates that there is a local vehicular component to the HCN measurement. Maximum HCN concentrations of 82 ppt on 4 November are higher than those associated with the regional signal (30–50 ppt). As the lifetime of NO is much less than HCN, the HCN/NO relationship is most obvious when wind speeds are low (typically $<3.0\ ms^{-1}$). As the wind speeds are higher on other weekdays, this is the most likely reason for poor correlations at those times. The example from 4 November indicates that a local enhancement of ~20 ppt is possible above the regional background. The maximum concentration associated with the BBP is 1.24 ppb, a factor of 10 higher than ambient.

For HNCO, the nonbonfire mean concentration is 12 ppt with a maximum of 144 ppt. Similarly to HCN, the strongest relationship between HNCO and NO is during rush hour on the low wind speed days of 4 and 5 November (R^2 = 0.71 and 0.72) but, unlike HCN, is poor on the other low wind speed days of 30 October and 7 November. A secondary source component to HNCO is evident as the HNCO/HCN ratio is higher in the presence of the photochemical marker ozone (Figure 5). One such formation pathway may be the oxidation of formamide (Borduas et al., 2015) with which HNCO has the highest correlation over the data set (R^2 = 0.71) (not including BBP). Further species with high correlations with HNCO are phenol (R^2 = 0.71), toluic acid (R^2 = 0.71), tartaric acid (R^2 = 0.70), and $C_5H_6O_2$ (R^2 = 0.70). The correlation between HCN and HNCO is good R^2 = 0.64. The maximum concentration measured during the bonfire plume of 1.64 ppb is comparable to concentrations recorded in agricultural burning plumes (Chandra & Sinha, 2016; Roberts et al., 2014) and is above the 1.0 ppb threshold, which is considered detrimental to human health (Roberts et al., 2011).

Maximum concentrations of MIC during the BBP of 4.3 ppb and 327 ppt outside of the BBP were observed. An R^2 of 0.75 with HCN and an of 0.53 with HNCO indicates that the behavior of MIC is more akin to HCN and is

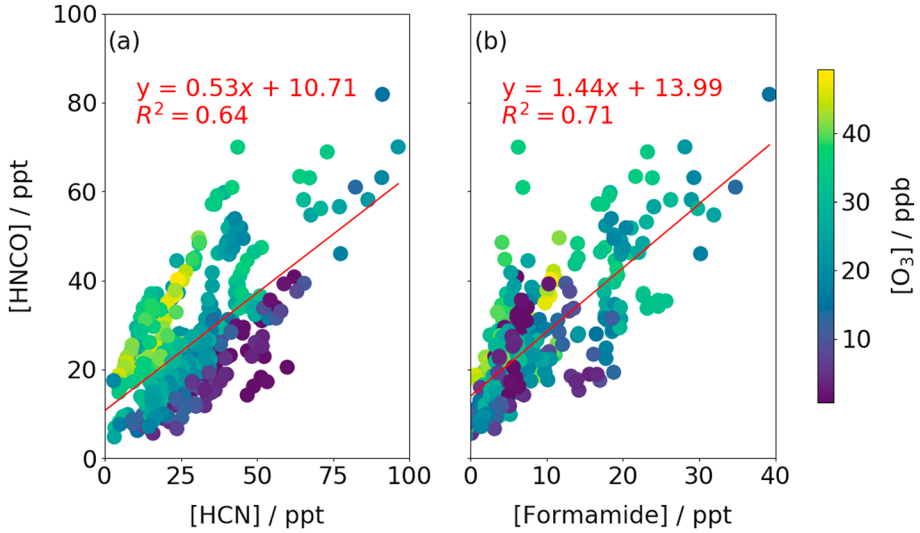

Figure 5. (a) HNCO versus HCN colored by levels of O_3. The photochemical component of the HNCO/HCN relationship is highlighted at high levels of O_3, which is indicative of photochemistry. (b) Positive relationship between formamide (HNCO precursor) and HNCO by levels of O_3. All data from the bonfire burn period has been removed (30 min average).

therefore more likely to be primary in origin. The diurnal profile of MIC shows a minimum in the early morning and large variation at rush hours consistent with typical NO_x diurnal profiles, indicating that MIC has a local, potentially traffic source.

We detect a large number of nitrates and nitrated species, some of which have been previously detected with CIMS (peroxynitric acid and PAN) and some that have not: nitroformic acid, nitroperoxy methane, and trinitrocyclohexane. The nitrates and nitrated species exhibit maxima during the day, yet elevated concentrations measured during the BBP are evident. Sharp increases in concentrations of all nitrates and nitrated species, similar to those of the isocyanate compounds, are observed, although the increase in ambient levels is not as high (factor of 3 compared with a factor of 10 for isocyanate compounds and HCN). Concentrations then increase again, later in the early morning of 6 November. Maximum PAN and trinitrocyclohexane concentrations of 221 and 133 ppt are measured at 16:00 on 31 October 2014, while during the bonfire plume the maximum concentrations are depleted to 15 and 73 ppt, respectively. Conversely, while high nitrophenol and methyl nitrophenol concentrations of 530 and 229 ppt are also recorded at other points in the measurement period (afternoon of 31 October 2014), the highest concentrations of 630 and 550 ppt are observed during the BBP. This BBP enhancement is short lived, however, with concentrations returning to ~300 ppt at 22:00.

Additional nitrogen-containing compounds were identified as amides: acrylamide, formamide, *N*-methylformamide, *N*,*N*-dimethylformamide, and *N*-formylformamide. Excluding the BBP, mean ambient concentrations are typically approximately tens of parts per thousand. Formamide, *N*-methylformamide, and *N*,*N*-dimethylformamide all exhibit maxima during the early afternoon (13:00–14:00) and minima during the morning rush hour (approximately 07:00–09:00). This is consistent with photochemical formation during the day and loss when NO_x concentrations are high. During the BBP, concentrations of all amide species increase to hundreds of parts per thousand very quickly. Unlike the nitrates, no secondary peaks in concentrations are detected later in the morning. Instead, concentrations return to ambient levels indicating that emission is short lived and loss processes are fast. These loss processes are unlikely to be homogeneous gas phase reactions as the lifetimes of these compounds, controlled by reaction with OH, are typically 1–2 days (Borduas et al., 2015; Bunkan et al., 2015).

3.3. Distinguishing Combustion Regimes and Emission Ratios.

Laboratory and field studies indicate that the ratio of [HNCOCO] decreases from 0.6–0.1% during flaming combustion to values 5–10 times lower during smoldering combustion (Roberts et al., 2010, 2011). By applying a 0.1% threshold, the criteria for flaming combustion is met between 17:30 and 20:00 on bonfire night.

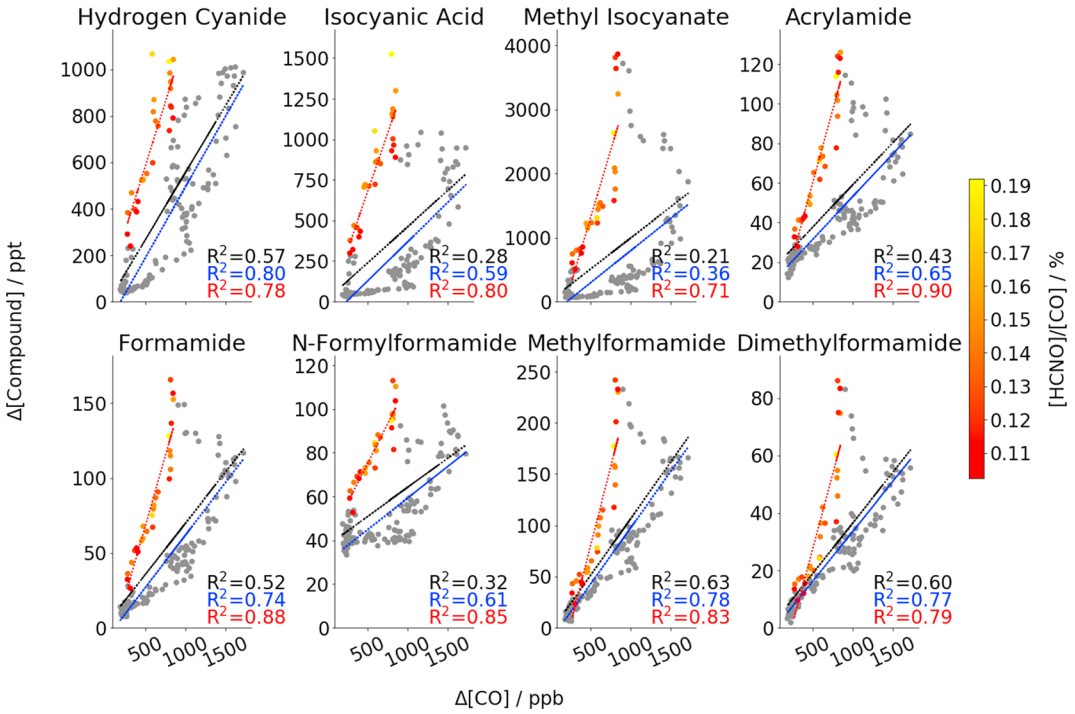

Figure 6. Normalized excess mixing ratios of selected compounds to CO. Gray points are smoldering phase emission described by the blue line, nongray points are flaming emission described by the red line, and black lines include all data. Slopes and R^2 are reported in Table 5.

This is the approximate time that most bonfire flaming combustion occurs, as previously stated. These times are indicative rather than exact, as there will be some variation in flaming time between events and air mass mixing will affect the temporal coincidence at the measurement site.

$$\mathrm{NEMR}_X = \frac{\Delta \boldsymbol{X}}{\Delta \mathrm{CO}} = \frac{X_{\mathrm{plume}} - X_{\mathrm{background}}}{\mathrm{CO}_{\mathrm{plume}} - \mathrm{CO}_{\mathrm{background}}} \quad (1)$$

The normalized excess mixing ratios (NEMRs) for a range of identified species relative to CO are calculated during the BBP using equation (1), many of which to the authors' knowledge have not previously been reported (Figure 6). The background concentrations of the species of interest and CO are taken as the mean value from the diurnal profile of that species and CO at 5 min time steps from the entire measurement period with the BBP removed. "Plume" concentrations of the species of interest and CO are taken

Table 5
Emission Ratios Relative to CO (ppt ppb^{-1})

	BBP		Flaming		Smoldering	
Compound	NEMR (ppt ppb^{-1})	R^2	NEMR (ppt ppb^{-1})	R^2	NEMR (ppt ppb^{-1})	R^2
Hydrogen cyanide	0.58 ± 0.68	0.57	1.11 ± 0.62	0.78	0.61 ± 0.31	0.80
Isocyanic acid	0.45 ± 0.96	0.28	1.44 ± 0.74	0.80	0.48 ± 0.40	0.59
Methyl isocyanate	0.97 ± 2.52	0.21	4.19 ± 2.81	0.71	1.00 ± 1.34	0.36
N-Formylformamide	0.03 ± 0.05	0.32	0.07 ± 0.03	0.85	0.03 ± 0.02	0.61
N,*N*-Dimethylformamide	0.04 ± 0.04	0.60	0.10 ± 0.06	0.79	0.03 ± 0.02	0.77
Acrylamide	0.04 ± 0.07	0.43	0.15 ± 0.05	0.90	0.04 ± 0.03	0.65
Formamide	0.07 ± 0.09	0.52	0.19 ± 0.07	0.88	0.07 ± 0.04	0.74
N-Methylformamide	0.11 ± 0.12	0.63	0.31 ± 0.15	0.83	0.11 ± 0.06	0.78

Note. Error reported is 2σ. BBP = bonfire burn period; NEMR = normalized excess mixing ratios.

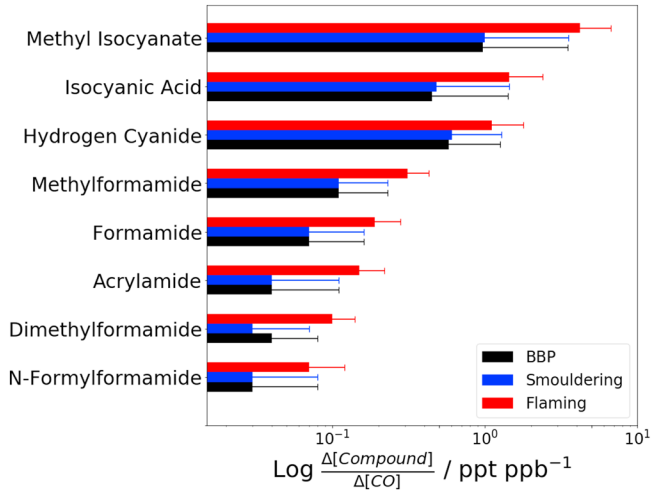

Figure 7. Normalized excess mixing ratio for HCN and seven selected isocyanate and amide compounds.

from the BBP. As bonfires are only lit after dark, photochemical production cannot occur during this time and so cannot confound any increases in measured concentrations.

By applying the [HNCOCO] metric to the NEMRs, it is possible to distinguish two distinct burning phases, flaming and smoldering (Figure 6). Table 5 and Figure 7 summarize the NEMRs for the identified species. Comparing the emission factor (EF) of a species as a function of the MCE (equation (2)) is best used to define the magnitude of emission during smoldering and flaming phase combustion (e.g., Yokelson et al., 1999).

$$\mathrm{MCE} = \frac{\Delta\ \mathrm{CO_2}}{\Delta\mathrm{CO} + \Delta\ \mathrm{CO_2}} \tag{2}$$

Calculating the MCE here is not possible as CO_2 was not measured; however, by using typical literature values of MCE where flaming and smoldering EF_{HCN} have been measured, it is possible to estimate the concentrations of CO_2 present due to BB. Using MCEs of 0.95 for flaming emission and 0.88 for smoldering emission (Akagi et al., 2013), we estimate that during flaming emission, CO_2 concentrations are 19 times greater than CO concentrations but only 7.3 times greater during smoldering emission. Using CO_2 + CO as a proxy for mass of material burned, 2.4 times more material was burned during the flaming phase than during smoldering. So while the NEMR appears greater for flaming emission than smoldering, it does not take into account the greater mass burned during the flaming emission stage. Normalizing the HCN NEMR to [CO_2] + [CO] (as a proxy for mass burned) for the different phases shows that the smoldering NEMR is higher than the flaming NEMR by about a third (32%) (S3).

In all instances, the correlation of the compound and CO during the entire BBP is less good than the correlations observed when the BBP is separated into the two different burn phases. This indicates that separating the BBP produces more accurate NEMRs. Errors during the smoldering emission phase are likely to be overestimated as they include the transition period from flaming to smoldering. Together, this indicates that the NEMR is underestimated, when considering the BBP as a whole, if flaming combustion is occurring and may lead to an artificial reduction in the perceived relationship of a species to a specific combustion phase. For example, the correlation of MIC and CO over the entire BBP is poor (R^2 = 0.21) indicating that there is a poor evidence for MIC emission during the BBP. However, if the burning phase is accounted for, the correlation during flaming emission is much higher (R^2 = 0.71) suggesting that a strong source of MIC emission is occurring during this flaming emission phase. The 2σ error on the MIC BBP regression is 259% of the slope value, yet the flaming phase error is 67%, again indicating that by considering the burn phase, the emission ratio is more accurate. Figure 7 shows that the NEMRs for HCN, HNCO, and MIC are approximately an order of magnitude higher than the amides, which to our knowledge represent the first reported NEMRs for these compounds.

The NEMR for HCN during flaming emission is 1.11 ± 0.62 ppt ppb^{-1} and is comparable to NEMRs from boreal forest fires in North America and Siberia (Tereszchuk et al., 2013); an agricultural building fire (Brilli et al., 2014); and African savannah, tropical, and extratropical forest fires (Hornbrook et al., 2011) but is low compared with other studies (Hornbrook et al., 2011, and references therein). Higher HCN NEMRs (5–12 ppt ppt^{-1}) have been detected in regions containing large cities where deposited NO_x contributes to the nitrogen enrichment of the emission from local forest fires (Yokelson et al., 2007), but as the fuels used in this instance are unlikely to have accumulated NO_x, this mechanism should not contribute to enhancing the nitrogen content of the fuel being burned.

Emissions of nitrogen-containing VOCs such as HCN and HNCO are known to be highly variable depending on the type and origin of the fuel. Increasing the nitrogen content of a biogenic fuel type by 1% can increase the emission of nitrogen-containing VOCs by 2–6% (Coggon et al., 2016), and the inclusion of a diesel oxidation catalyst to a diesel engine can increase the HNCO NEMR by a factor of 30 (Jathar et al., 2017). Total isocyanate concentrations measured after burning various plastics can vary by 3 orders of magnitude

Table 6
Maximum Concentrations of Routinely Measured Pollutants Measured at the Whitworth Observatory With Their Respective NAQO

			Bonfire measurements 29/10/2014 to 11/11/2014		From 1/6/2014 to 28/2/2016 (includes bonfire night)	
Pollutant	NAQO (ppb)	Sample period	C_{max} (ppb)	Time	C_{max} (ppb)	Time
NO_2	105	1 h mean	46.76	5/11/2014 19:00	60.79	3/12/2014 17:00
SO_2	132	1 h mean	1.78	5/11/2014 20:00	14.82	21/9/2014 12:00
SO_2	47	24 h mean	0.69	9/11/2014	3.32	21/9/2014
CO	8,377	8 h running mean	1,551.78	5/11/2014 21:00	1,551.78	5/11/2014 21:00

Note. Dates are formatted as day/month/year. NAQO = UK National Air Quality Objectives.

depending on the precursor fuel nitrogen content, and accordingly, plastics containing no nitrogen do not produce any isocyanates (Blomqvist et al., 2003). This variability in fuel type is one potential reason that the HCN NEMR is low. Another reason may be the assumption that the enhancement in CO above the calculated background is entirely due to bonfire burning is not accurate enough, as other sources of CO, for example, fireworks and or enhanced contribution from cars, cause an underestimation in the NEMR. Unfortunately, no discernable tracer of firework activity was found using iodide CIMS. During street to city-scale dispersion experiments over (approximately) 2–5 km, using inert perflurocarbon gas tracers, the ratio of different tracers released at the same point remained constant over all distances measured (Martin et al., 2010, 2011; Wood et al., 2009). Depending on the prevailing wind speed, the tracer ratio did not return to background levels following cessation of tracer release for 30–60 min at the release point itself. In other experiments where inert tracer was heated to produce a buoyant plume, not only was it detected at much further distances downwind, the ratio was also preserved (Britter et al., 2002). While multiple sources will inevitably have different initial ratios (e.g., [HNCOCO]), those ratios should be preserved over at least kilometer-scale distances. It is impossible of course to categorically define the transition from a flaming phase to a smoldering phase, but given the very long lifetime of HNCO and CO with respect to travel time (based on when fires are likely to have been lit) the two distinct phases identified should be robust.

3.4. Air Quality

The highest concentration of CO recorded during the BBP is 1,551 ppb (as an 8 h running mean) which is comparable with summertime pollution events in London (Bannan et al., 2014). A maximum NO_2 concentration of 43.76 ppb is measured during the BBP. Of the pollutants routinely measured at the Whitworth Observatory, none of the UK National Air Quality Objectives (NAQOs) (Defra, 2012) were breached during the measurement period at this measurement site. The highest maximum recorded concentrations of the pollutants at their NAQO sample periods were between 19:00 and 21:00 on bonfire night except the 24 h mean SO_2, which occurred 4 days later.

As the Whitworth Observatory is approximately 15 m above ground level and 100 m from the nearest road, it is not considered a roadside/kerbside site, and so these data cannot convey any enhancement in concentration due to local vehicular emission at roadside where pollution levels and human exposure are often highest. However, this analysis does demonstrate that NO_2 and SO_2 concentrations are higher at times in the year other than bonfire night due to other phenomena, typically local traffic emission at times of low wind speed. Although the SO_2 concentrations at their highest are much lower than the NAQOs, NO_2 concentrations are noteworthy (Table 6).

3.5. Health Impacts

It is difficult to translate concentrations of the trace gas species measured with the ToF-CIMS into impacts on human health. Attention has mainly focused on particulate matter, NO_2, CO, SO_2, and O_3. In a comprehensive review of the literature on the human impact of wildland fire smoke, which shares some of its source materials with what is burnt during bonfire night, consistent associations with mortality and respiratory morbidity were observed (Liu et al., 2015), although most of these wildfires would occur for longer periods than the one night evaluated here. Adetona et al. (2016) similarly concluded that for the general (exposed) public there was strong evidence of an association with acute respiratory effects,

weak evidence of acute cardiovascular effects and insufficient evidence for any conclusions regarding birth outcomes. In an attempt to put the findings of this study in context, we use the risk communication methodology of van der Zee et al. (2016) to communicate the risk from specific air pollutants in equivalent numbers of passively smoked cigarettes.

The maximum 1 h mean NO_2 concentration encountered during the 2014 Bonfire night was 46.76 ppb, which, although below air quality limits, is approximately 13.82 ppb above the estimated regional concentration above the surface layer for 2014 in Manchester (Defra, 2017). The 1 h mean concentration of black carbon fluctuated between 0 and 5 $\mu g\ m^{-3}$ during the measurement period but increased to its maximum of 21.11 $\mu g\ m^{-3}$ during bonfire night. The average concentrations of these two pollutants from 16:00 to 04:00 over bonfire night are estimated to be the equivalent to 26.1 passively smoked cigarettes.

The methodology described here, however, additionally identified trace amounts of many other chemicals generally not measured, many of which are known irritants and/or toxicants at higher (ppm) exposure levels: for example, in terms of workplace limit values MIC has a threshold limit value of 0.2 ppm (National Institute for Occupational Safety and Health, 2017), the Occupational Safety and Health Administration permissible exposure limit for HCN is 10 ppm (time weighted average) or 5 mg/m^3 averaged over 15 min (U.S. Department of Labor, 2005) and may be carcinogenic or teratogenic. However, the health impact of these chemicals at the low parts per billion level at which they are observed here remains unknown, if any given the likely duration during which human exposure would occur.

4. Conclusions

Here we present the first simultaneous online gas phase measurements of isocyanates, amides, and nitrates and nitro-organics using the ToF-CIMS during a 2 week period including bonfire night (5 November) and present, to our knowledge, the first reported NEMRs of amides to CO.

Typical HCN concentrations of 0–50 ppt were measured before and after bonfire night with a maximum of 82 ppt measured during rush hours when wind speeds were low. Mean HNCO concentrations were 12 ppt, and a maximum of 144 ppt was measured at the same time as high HCN concentrations. While HNCO concentrations show evidence of a photochemical source, MIC does not and behaves more like HCN as a primary pollutant. Maximum bonfire night concentrations of HCN and HNCO were 1.24 ppb and 1.64 ppb, respectively. Nitrates, nitrated species, and amide enhancements were lower than those for HCN and HNCO at ~2–3.5 times higher than ambient levels.

No one bonfire was directly sampled as a shallow inversion layer, and low wind speeds caused a pooling of outflow from many large- and small-scale emission sources. We identify that the bonfire burn period (BBP) lasted between approximately 16:00 and 04:00–05:00 when using HCN as a tracer. No tracer for fireworks was found using iodide CIMS.

In the absence of CO_2 measurements and therefore MCE calculations, we use a HNCO:CO ratio of 0.1% to distinguish flaming and smoldering combustion (Roberts et al., 2011) and report normalized excess mixing ratios (NEMRs) relative to CO for HCN and a range of isocyanates and amides, many of which have not been reported before. The NEMRs separated by combustion phase are more accurate than when treating the BBP as a whole, with flaming phase showing greater enhancements than smoldering. We note that this does not take into account the amount of mass burned. The flaming phase NEMR of HCN = 1.11 ± 0.62 ppt ppb^{-1}, while low is consistent with other studies of biogenic BB (e.g., Tereszchuk et al., 2013). The uncertainty of the mixed fuel types used in bonfire construction prevents a detailed analysis of whether fuel nitrogen content is consistent with this lower HCN NEMR. Future work should attempt to better understand the composition of the mixed fuel types used in anthropogenic open burning.

The highest concentration of CO at this measurement site within a year and a half period (inclusive of this data) was measured during bonfire night, further confirming that this is a high-pollution event, yet match those measured in London during summer (Bannan et al., 2014). Conversely, NO_2 concentrations were higher at other times within that year and a half period at this site, indicating that other phenomena can contribute more than bonfire night to increased levels of NO_2. NO_2 concentrations measured here do not exceed current national air quality objectives (NAQOs) but equally do not represent kerbside measurements where the majority of NO_2 exceedances occur (McLean & Drabble, 2015).

The health impact of the exposures to the many identified chemicals in the parts per thousand range is unknown, although maximum 1 min average concentrations of HNCO during the BBP exceed 1 ppb, which has previously been considered above levels harmful to humans (Roberts et al., 2011). Initial assessment of a combination of black carbon and NO_2 indicates that this exposure, at the measurement location, would be equivalent to an average of 26.1 passively smoked cigarettes between 16:00 and 04:00 during bonfire night. As detection of toxic compounds becomes more routine, their inclusion in health burden quantification methodologies would further contribute to understanding the true impact of BB events on human health.

Acknowledgments
This work was supported by the EAO NERC DTP. D. E. S. and M. A. H. K. would like to thank NERC (NE/K01501X). Processed data are available via the British Atmospheric Data Centre (BADC) http://catalogue.ceda.ac.uk/uuid/71a34def1d104f1e925f1a6f7-d12ac21, are archived at the University of Manchester, and are available on request.

References

Adetona, O., Reinhardt, T. E., Domitrovich, J., Broyles, G., Adetona, A. M., Kleinman, M. T., et al. (2016). Review of the health effects of wildland fire smoke on wildland firefighters and the public. *Inhalation Toxicology*, *28*(3), 95–139. https://doi.org/10.3109/08958378.2016.1145771

Akagi, S. K., Yokelson, R. J., Burling, I. R., Meinardi, S., Simpson, I., Blake, D. R., et al. (2013). Measurements of reactive trace gases and variable O_3 formation rates in some South Carolina biomass burning plumes. *Atmospheric Chemistry and Physics*, *13*(3), 1141–1165. https://doi.org/10.5194/acp-13-1141-2013

Akagi, S. K., Yokelson, R. J., Wiedinmyer, C., Alvarado, M. J., Reid, J. S., Karl, T., et al. (2011). Emission factors for open and domestic biomass burning for use in atmospheric models. *Atmospheric Chemistry and Physics*, *11*(9), 4039–4072. Retrieved from http://www.atmos-chem-phys.net/11/4039/2011/, https://doi.org/10.5194/acp-11-4039-2011

Amann, M., Purohit, P., Bhanarkar, A. D., Bertok, I., Borken-Kleefeld, J., Cofala, J., et al. (2017). Managing future air quality in megacities: A case study for Delhi. *Atmospheric Environment*, *161*, 99–111. Retrieved from http://linkinghub.elsevier.com/retrieve/pii/S1352231017302856, https://doi.org/10.1016/j.atmosenv.2017.04.041

Ambrose, J. L., Zhou, Y., Haase, K., Mayne, H. R., Talbot, R., & Sive, B. C. (2012). A gas chromatographic instrument for measurement of hydrogen cyanide in the lower atmosphere. *Atmospheric Measurement Techniques*, *5*(6), 1229–1240. Retrieved from http://www.atmos-meas-tech.net/5/1229/2012/, https://doi.org/10.5194/amt-5-1229-2012

Andreae, M. O., & Merlet, P. (2001). Emission of trace gases and aerosols from biomass burning. *Global Biogeochemical Cycles*, *15*(4), 955–966. https://doi.org/10.1029/2000GB001382

Bannan, T. J., Bacak, A., Muller, J. B. A., Booth, A. M., Jones, B., le Breton, M., et al. (2014). Importance of direct anthropogenic emissions of formic acid measured by a chemical ionisation mass spectrometer (CIMS) during the winter ClearfLo campaign in London, January 2012. *Atmospheric Environment*, *83*, 301–310. https://doi.org/10.1016/j.atmosenv.2013.10.029

Bannan, T. J., Booth, A. M., Bacak, A., Muller, J. B. A., Leather, K. E., Le Breton, M., et al. (2015). The first UK measurements of nitryl chloride using a chemical ionisation mass spectrometer in central London in the summer of 2012, and an investigation of the role of Cl atom oxidation. *Journal of Geophysical Research: Atmospheres*, *120*, 5638–5657. https://doi.org/10.1002/2014JD022629

Bannan, T. J., Booth A. M., Jones B. T., O'Meara S., Barley M. H., Riipinen I., et al. (2017). Measured saturation vapor pressures of phenolic and nitro-aromatic compounds. *Environmental Science & Technology*, *51*(7) 3922–3928. https://doi.org/10.1021/acs.est.6b06364

Berndt, T., & Böge, O. (2006). Formation of phenol and carbonyls from the atmospheric reaction of OH radicals with benzene. *Physical Chemistry Chemical Physics (PCCP)*, *8*(10), 1205–1214. https://doi.org/10.1039/b514148f

Bertram, T. H., Thornton, J. A., & Riedel, T. P. (2009). An experimental technique for the direct measurement of N_2O_5 reactivity on ambient particles. *Atmospheric Measurement Techniques*, *2*(1), 231–242. Retrieved from www.atmos-meas-tech.net/2/231/2009/, https://doi.org/10.5194/amt-2-231-2009

Blomqvist, P., Hertzberg, T., Dalene, M., & Skarping, G. (2003). Isocyanates, aminoisocyanates and amines from fires—A screening of common materials found in buildings. *Fire and Materials*, *27*(6), 275–294. https://doi.org/10.1002/fam.836

Bonde, J. P., Flachs, E. M., Rimborg, S., Glazer, C. H., Giwercman, A., Ramlau-Hansen, C. H., et al. (2016). The epidemiologic evidence linking prenatal and postnatal exposure to endocrine disrupting chemicals with male reproductive disorders: A systematic review and meta-analysis. *Human Reproduction Update (Hypothesis)*, *4*, 1–22.

Borduas, N., da Silva, G., Murphy, J. G., & Abbatt, J. P. D. (2015). Experimental and theoretical understanding of the gas phase oxidation of atmospheric amides with OH radicals: Kinetics, products, and mechanisms. *Journal of Physical Chemistry A*, *119*(19), 4298–4308. https://doi.org/10.1021/jp503759f

Borduas, N., Place, B., Wentworth, G. R., Abbatt, J. P. D., & Murphy, J. G. (2016). Solubility and reactivity of HNCO in water: Insights into HNCO's fate in the atmosphere. *Atmospheric Chemistry and Physics*, *16*(2), 703–714. https://doi.org/10.5194/acp-16-703-2016

Brilli, F., Gioli, B., Ciccioli, P., Zona, D., Loreto, F., Janssens, I. A., & Ceulemans, R. (2014). Proton transfer reaction time-of-flight mass spectrometric (PTR-TOF-MS) determination of volatile organic compounds (VOCs) emitted from a biomass fire developed under stable nocturnal conditions. *Atmospheric Environment*, *97*, 54–67. https://doi.org/10.1016/j.atmosenv.2014.08.007

Bristow, A. W. T., & Webb, K. S. (2003). Intercomparison study on accurate mass measurement of small molecules in mass spectrometry. *Journal of the American Society for Mass Spectrometry*, *14*(10), 1086–1098. https://doi.org/10.1016/S1044-0305(03)00403-3

Brophy, P., & Farmer, D. K. (2015). A switchable reagent ion high resolution time-of-flight chemical ionization mass spectrometer for real-time measurement of gas phase oxidized species: Characterization from the 2013 southern oxidant and aerosol study. *Atmospheric Measurement Techniques*, *8*(7), 2945–2959. Retrieved from http://www.atmos-meas-tech.net/8/2945/2015/, https://doi.org/10.5194/amt-8-2945-2015

Bunkan, A. J. C., Hetzler, J., Mikoviny, T., Wisthaler, A., Nielsen, C. J., & Olzmann, M. (2015). The reactions of *N*-methylformamide and *N,N*-dimethylformamide with OH and their photo-oxidation under atmospheric conditions: Experimental and theoretical studies. *Physical Chemistry Chemical Physics (PCCP)*, *17*(10), 7046–7059. Retrieved from http://pubs.rsc.org/en/content/articlehtml/2015/cp/c4cp05805d, https://doi.org/10.1039/C4CP05805D

Caird, S., Roy, R., & Herring, H. (2008). Improving the energy performance of UK households: Results from surveys of consumer adoption and use of low- and zero-carbon technologies. *Energy Efficiency*, *1*(2), 149–166. https://doi.org/10.1007/s12053-008-9013-y

Chandra, B. P., & Sinha, V. (2016). Contribution of post-harvest agricultural paddy residue fires in the N.W. Indo-Gangetic Plain to ambient carcinogenic benzenoids, toxic isocyanic acid and carbon monoxide. *Environment International*, *88*, 187–197. https://doi.org/10.1016/j.envint.2015.12.025

Chhabra, P. S., Lambe, A. T., Canagaratna, M. R., Stark, H., Jayne, J. T., Onasch, T. B., et al. (2015). Application of high-resolution time-of-flight chemical ionization mass spectrometry measurements to estimate volatility distributions of α-pinene and naphthalene oxidation

products. *Atmospheric Measurement Techniques*, *8*(1), 1–18. Retrieved from http://www.atmos-meas-tech.net/8/1/2015/, https://doi.org/10.5194/amt-8-1-2015

Coggon, M. M., Veres, P. R., Yuan, B., Koss, A., Warneke, C., Gilman, J. B., et al. (2016). Emissions of nitrogen-containing organic compounds from the burning of herbaceous and arboraceous biomass: Fuel composition dependence and the variability of commonly used nitrile tracers. *Geophysical Research Letters*, *43*, 9903–9912. https://doi.org/10.1002/2016GL070562

Defra (2012). National air quality objectives. Retrieved from https://uk-air.defra.gov.uk/assets/documents/National_air_quality_objectives.pdf, Accessed April 20, 2017.

Defra (2017). Background maps. Retrieved from https://uk-air.defra.gov.uk/data/laqm-background-home, Accessed February 23, 2017.

Drewnick, F., Hings, S. S., Curtius, J., Eerdekens, G., & Williams, J. (2006). Measurement of fine particulate and gas-phase species during the new year's fireworks 2005 in Mainz, Germany. *Atmospheric Environment*, *40*(23), 4316–4327. Retrieved from http://www.sciencedirect.com/science/article/pii/S1352231006003499, https://doi.org/10.1016/j.atmosenv.2006.03.040

Dyke, P., Coleman, P., & James, R. (1997). Dioxins in ambient air, bonfire night 1994. *Chemosphere*, *34*(5–7), 1191–1201. https://doi.org/10.1016/S0045-6535(97)00418-9

Ehn, M., Thornton, J. A., Kleist, E., Sipilä, M., Junninen, H., Pullinen, I., et al. (2014). A large source of low-volatility secondary organic aerosol. *Nature*, *506*(7489), 476–479. https://doi.org/10.1038/nature13032/npapers2://publication/doi/10.1038/nature13032

Farrar, N. J., Smith, K. E. C., Lee, R. G. M., Thomas, G. O., Sweetman, A. J., & Jones, K. C. (2004). Atmospheric emissions of polybrominated diphenyl ethers and other persistent organic pollutants during a major anthropogenic combustion event. *Environmental Science and Technology*, *38*(6), 1681–1685. https://doi.org/10.1021/es035127d

Fuller, G. W., Tremper, A. H., Baker, T. D., Yttri, K. E., & Butterfield, D. (2014). Contribution of wood burning to PM_{10} in London. *Atmospheric Environment*, *87*, 87–94. https://doi.org/10.1016/j.atmosenv.2013.12.037

Gescher, A. (1990). 2.3 - Formamide A2 - BUHLER, D.R. In D. J. B. T.-N. And P. S (Ed.), *Ethel Browning's toxicity and metabolism of industrial solvents*, (Second E. REED ed.pp. 160–164). Amsterdam: Elsevier. Retrieved from http://www.sciencedirect.com/science/article/pii/B9780444813169500311

Harrad, S. J., & Laurie, L. (2005). Concentrations, sources and temporal trends in atmospheric polycyclic aromatic hydrocarbons in a major conurbation. *Journal of Environmental Monitoring*, *7*(7), 722–727. https://doi.org/10.1039/b503983e

Harrison, T., & Shallcross, D. E. (2011). Smoke is in the air: How fireworks affect air quality Did you realise that fireworks cause measurable air pollution? *Science in School*, *21*, 47–51.

Henriks-Eckerman, M.-L., Välimaa, J., Rosenberg, C., Peltonen, K., & Engström, K. (2002). Exposure to airborne isocyanates and other thermal degradation products at polyurethane-processing workplaces. *Journal of Environmental Monitoring*, *4*(5), 717–721. Retrieved from http://xlink.rsc.org/?DOI=b206339p. https://doi.org/10.1039/B206339P

Hornbrook, R. S., Blake, D. R., Diskin, G. S., Fried, A., Fuelberg, H. E., Meinardi, S., et al. (2011). Observations of nonmethane organic compounds during ARCTAS—Part 1: Biomass burning emissions and plume enhancements. *Atmospheric Chemistry and Physics*, *11*(21), 11,103–11,130. https://doi.org/10.5194/acp-11-11103-2011

Iinuma, Y., Böge, O., & Herrmann, H. (2010). Methyl-nitrocatechols: Atmospheric tracer compounds for biomass burning secondary organic aerosols. *Environmental Science and Technology*, *44*(22), 8453–8459. https://doi.org/10.1021/es102938a

Iyer, S., Lopez-Hilfiker F., Lee B. H., Thornton, J. A., & Kurtén T. (2016). Modeling the detection of organic and inorganic compounds using iodide-based chemical ionization. *The Journal of Physical Chemistry A*, *120*(4), 576–587. https://doi.org/10.1021/acs.jpca.5b09837

Jathar, S. H., Heppding, C., Link, M. F., Farmer, D. K., Akherati, A., Kleeman, M. J., et al. (2017). Investigating diesel engines as an atmospheric source of isocyanic acid in urban areas. *Atmospheric Chemistry and Physics*, *17*(14), 8959–8970. https://doi.org/10.5194/acp-17-8959-2017

Junninen, H., Ehn, M., Petäjä, T., Luosujärvi, L., Kotiaho, T., Kostiainen, R., et al. (2010). A high-resolution mass spectrometer to measure atmospheric ion composition. *Atmospheric Measurement Techniques*, *3*(4), 1039–1053. Retrieved from http://www.atmos-meas-tech.net/3/1039/2010/, https://doi.org/10.5194/amt-3-1039-2010

Kim, K. H., Pandey, S. K., Kim, Y. H., Sohn, J. R., & Oh, J. M. (2015). Emissions of amides (*N*,*N*-dimethylformamide and formamide) and other obnoxious volatile organic compounds from different mattress textile products. *Ecotoxicology and Environmental Safety*, *114*, 350–356. https://doi.org/10.1016/j.ecoenv.2014.07.008

Knighton, W. B., Fortner, E. C., Midey, A. J., Viggiano, A. A., Herndon, S. C., Wood, E. C., & Kolb, C. E. (2009). HCN detection with a proton transfer reaction mass spectrometer. *International Journal of Mass Spectrometry*, *283*(1–3), 112–121. https://doi.org/10.1016/j.ijms.2009.02.013

Le Breton, M., Bacak, A., Muller, J. B. A., O'Shea, S. J., Xiao, P., Ashfold, M. N. R., et al. (2013). Airborne hydrogen cyanide measurements using a chemical ionisation mass spectrometer for the plume identification of biomass burning forest fires. *Atmospheric Chemistry and Physics*, *13*(18), 9217–9232. https://doi.org/10.5194/acp-13-9217-2013

Le Breton, M., Bacak, A., Muller, J. B. A., Bannan, T. J., Kennedy, O., Ouyang, B., et al. (2014). The first airborne comparison of N_2O_5 measurements over the UK using a CIMS and BBCEAS during the RONOCO campaign. *Analytical Methods*, *6*(24), 9731–9743. Retrieved from http://pubs.rsc.org/en/content/articlehtml/2014/ay/c4ay02273d, https://doi.org/10.1039/C4AY02273D

Le Breton, M., McGillen, M. R., Muller, J. B. A., Bacak, A., Shallcross, D. E., Xiao, P., et al. (2012). Airborne observations of formic acid using a chemical ionization mass spectrometer. *Atmospheric Measurement Techniques*, *5*(12), 3029–3039.

Leather, K. E., McGillen, M. R., & Percival, C. J. (2010). Temperature-dependent ozonolysis kinetics of selected alkenes in the gas phase: An experimental and structure-activity relationship (SAR) study. *Physical Chemistry Chemical Physics (PCCP)*, *12*(12), 2935–2943. https://doi.org/10.1039/b919731a

Lee, B. H., Lopez-Hilfiker, F. D., Mohr, C., Kurtén, T., Worsnop, D. R., & Thornton, J. A. (2014). An iodide-adduct high-resolution time-of-flight chemical-ionization mass spectrometer: Application to atmospheric inorganic and organic compounds. *Environmental Science & Technology*, *48*(11), 6309–6317. https://doi.org/10.1021/es500362a

Li, Q., Jacob, D. J., Yantosca, R. M., Heald, C. L., Singh, H. B., Koike, M., et al. (2003). A global three-dimensional model analysis of the atmospheric budgets of HCN and CH_3CN: Constraints from aircraft and ground measurements. *Journal of Geophysical Research*, *108*(D21), 8827. https://doi.org/10.1029/2002JD003075

Li, Q., Palmer, P. I., Pumphrey, H. C., Bernath, P., & Mahieu, E. (2009). What drives the observed variability of HCN in the troposphere and lower stratosphere? *Atmospheric Chemistry and Physics*, *9*(21), 8531–8543. Retrieved from http://www.atmos-chem-phys.net/9/8531/2009/, https://doi.org/10.5194/acp-9-8531-2009

Liu, J. C., Pereira, G., Uhl, S. A., Bravo, M. A., & Bell, M. L. (2015). A systematic review of the physical health impacts from non-occupational exposure to wildfire smoke. *Environmental Research*, *136*, 120–132. https://doi.org/10.1016/j.envres.2014.10.015

Lopez-Hilfiker, F. D., Iyer, S., Mohr, C., Lee, B. H., D'Ambro, E. L., Kurtén, T., & Thornton, J. A. (2015). Constraining the sensitivity of iodide adduct chemical ionization mass spectrometry to multifunctional organic molecules using the collision limit and thermodynamic stability of

iodide ion adducts. *Atmospheric Measurement Techniques Discussions*, *8*(10), 10,875–10,896. Retrieved from http://www.atmos-meas-tech-discuss.net/8/10875/2015/, https://doi.org/10.5194/amtd-8-10875-2015

Lu, Z., Hebert, V. R., & Miller, G. C. (2014). Gas-phase reaction of methyl isothiocyanate and methyl isocyanate with hydroxyl radicals under static relative rate conditions. *Journal of Agricultural and Food Chemistry*, *62*(8), 1792–1795. Retrieved from http://www.ncbi.nlm.nih.gov/pubmed/24483206

Lüttke, J., Scheer, V., Levsen, K., Wünsch, G., Neil Cape, J., Hargreaves, K. J., et al. (1997). Occurrence and formation of nitrated phenols in and out of cloud. *Atmospheric Environment*, *31*(16), 2637–2648. https://doi.org/10.1016/S1352-2310(96)00229-4

Mari, M., Harrison, R. M., Schuhmacher, M., Domingo, J. L., & Pongpiachan, S. (2010). Inferences over the sources and processes affecting polycyclic aromatic hydrocarbons in the atmosphere derived from measured data. *Science of the Total Environment*, *408*(11), 2387–2393. https://doi.org/10.1016/j.scitotenv.2010.01.054

Martin, D., Petersson, K. F., & Shallcross, D. E. (2011). The use of cyclic perfluoroalkanes and SF6 in atmospheric dispersion experiments. *Quarterly Journal of the Royal Meteorological Society*, *137*(661), 2047–2063.

Martin, D., Price, C. S., White, I. R., Nickless, G., Petersson, K. F., Britter, R. E., et al. (2010). Urban tracer dispersion experiments during the second DAPPLE field campaign in London 2004. *Atmospheric Environment*, *44*(25), 3043–3052.

McLean, A. & Drabble, J. (2015). 2014 detailed air quality assessment for Greater Manchester The Greater Manchester Combined Authority. Retrieved from http://www.manchester.gov.uk/downloads/download/4166/air_quality_reports

Mohr, C., Lopez-Hilfiker, F. D., Zotter, P., Prévôt, A. S., Xu, L., Ng, N. L., et al. (2013). Contribution of nitrated phenols to wood burning Brown carbon light absorption in Detling, United Kingdom during winter time. *Environmental Science & Technology*, *47*(12), 6316–6324. https://doi.org/10.1021/es400683v

Molina, L. T., Kolb, C. E., de Foy, B., Lamb, B. K., Brune, W. H., Jimenez, J. L., et al. (2007). Air quality in North America's most populous city–overview of the MCMA-2003 campaign. *Atmospheric Chemistry and Physics*, *7*(10), 2447–2473. https://doi.org/10.5194/acp-7-2447-2007

Moreno, T., Querol, X., Alastuey, A., Cruz Minguillón, M., Pey, J., Rodriguez, S., et al. (2007). Recreational atmospheric pollution episodes: Inhalable metalliferous particles from firework displays. *Atmospheric Environment*, *41*(5), 913–922. Retrieved from http://linkinghub.elsevier.com/retrieve/pii/S1352231006009745, https://doi.org/10.1016/j.atmosenv.2006.09.019

Mouly, T. A., & Toms, L. L. (2016). Breast cancer and persistent organic pollutants (excluding DDT): A systematic literature review. *Environmental Science and Pollution Research*, *23*(22), 22,385–22,407. https://doi.org/10.1007/s11356-016-7577-1

Moussa, S. G., Leithead, A., Li, S.-M., Chan, T. W., Wentzell, J. J. B., Stroud, C., et al. (2016). Emissions of hydrogen cyanide from on-road gasoline and diesel vehicles. *Atmospheric Environment*, *131*, 185–195. https://doi.org/10.1016/j.atmosenv.2016.01.050

Nadal, M., Marquès, M., Mari, M., & Domingo, J. L. (2015). Climate change and environmental concentrations of POPs: A review. *Environmental Research*, *143*, 177–185. https://doi.org/10.1016/j.envres.2015.10.012

National Institute for Occupational Safety and Health (2017). CDC—Benzoic acid—International Chemical Safety Cards - NIOSH. Retrieved from https://www.cdc.gov/niosh/ipcsneng/neng0103.html

Pongpiachan, S., Tipmanee, D., Khumsup, C., Kittikoon, I., & Hirunyatrakul, P. (2015). Assessing risks to adults and preschool children posed by $PM_{2.5}$-bound polycyclic aromatic hydrocarbons (PAHs) during a biomass burning episode in northern Thailand. *Science of the Total Environment*, *508*, 435–444. https://doi.org/10.1016/j.scitotenv.2014.12.019

Reyes-Villegas, E., Priestley, M., Ting, Y. C., Haslett, S., Bannan, T., le Breton, M., et al. (2017). Supplemental information for: Simultaneous aerosol mass spectrometry and chemical ionisation mass spectrometry measurements during a biomass burning event in the UK: Insights into nitrate chemistry. *Atmospheric Chemistry and Physics Discussions*, (July), 1–22. https://doi.org/10.5194/acp-2017-605

Roberts, J. M., Veres, P., Warneke, C., Neuman, J. A., Washenfelder, R. A., Brown, S. S., et al. (2010). Measurement of HONO, HNCO, and other inorganic acids by negative-ion proton-transfer chemical-ionization mass spectrometry (NI-PT-CIMS): Application to biomass burning emissions. *Atmospheric Measurement Techniques*, *3*(4), 981–990. https://doi.org/10.5194/amt-3-981-2010

Roberts, J. M., Veres, P. R., Cochran, A. K., Warneke, C., Burling, I. R., Yokelson, R. J., et al. (2011). Isocyanic acid in the atmosphere and its possible link to smoke-related health effects. *Proceedings of the National Academy of Sciences of the United States of America*, *108*(22), 8966–8971. https://doi.org/10.1073/pnas.1103352108

Roberts, J. M., Veres, P. R., VandenBoer, T. C., Warneke, C., Graus, M., Williams, E. J., et al. (2014). New insights into atmospheric sources and sinks of isocyanic acid, HNCO, from recent urban and regional observations. *Journal of Geophysical Research: Atmospheres*, *119*, 1060–1072. https://doi.org/10.1002/2013JD019931

Sarkar, C., Sinha, V., Kumar, V., Rupakheti, M., Panday, A., Mahata, K. S., et al. (2016). Overview of VOC emissions and chemistry from PTR-TOF-MS measurements during the SusKat-ABC campaign: High acetaldehyde, isoprene and isocyanic acid in wintertime air of the Kathmandu Valley. *Atmospheric Chemistry and Physics*, *16*(6), 3979–4003. https://doi.org/10.5194/acp-16-3979-2016

Sarkar, C., Sinha, V., Sinha, B., Panday, A. K., Rupakheti, M., & Lawrence, M. G. (2017). Source apportionment of NMVOCs in the Kathmandu Valley during the SusKat-ABC international field campaign using positive matrix factorization. *Atmospheric Chemistry and Physics*, *17*(13), 8129–8156. https://doi.org/10.5194/acp-17-8129-2017

Sekler, M. S., Levi, Y., Polyak, B., Novoa, A., Dunlop, P. S. M., Byrne, J. A., & Marks, R. S. (2004). Monitoring genotoxicity during the photocatalytic degradation of *p*-nitrophenol. *Journal of Applied Toxicology*, *24*(5), 395–400. https://doi.org/10.1002/jat.1029

Shim, C., Wang, Y., Singh, H. B., Blake, D. R., & Guenther, A. B. (2007). Source characteristics of oxygenated volatile organic compounds and hydrogen cyanide. *Journal of Geophysical Research*, *112*, D10305. https://doi.org/10.1029/2006JD007543

Stockwell, C. E., Veres, P. R., Williams, J., & Yokelson, R. J. (2015). Characterization of biomass burning emissions from cooking fires, peat, crop residue, and other fuels with high-resolution proton-transfer-reaction time-of-flight mass spectrometry. *Atmospheric Chemistry and Physics*, *15*(2), 845–865. Retrieved from http://www.atmos-chem-phys.net/15/845/2015/, https://doi.org/10.5194/acp-15-845-2015

Tereszchuk, K. A., González Abad, G., Clerbaux, C., Hadji-Lazaro, J., Hurtmans, D., Coheur, P. F., & Bernath, P. F. (2013). ACE-FTS observations of pyrogenic trace species in boreal biomass burning plumes during BORTAS. *Atmospheric Chemistry and Physics*, *13*(9), 4529–4541. https://doi.org/10.5194/acp-13-4529-2013

U.S. Department of Labor (2005). Chemical sampling information | chlorobenzene | occupational safety and health administration., P. Accessed 23/02/2017. Retrieved from https://www.osha.gov/dts/chemicalsampling/data/CH_227000.html

UK Government, D. for C. and L. (2015). Celebrating with bonfires and fireworks. Retrieved from https://www.gov.uk/government/publications/burning-of-waste-on-campfires-and-bonfires

United Nations (2016). The world's cities in 2016—Data booklet (ST/ESA/ SER.A/392). *The World's Cities in 2016*. Retrieved from www.unpopulation.org.

van der Zee, S. C., Fischer, P. H., & Hoek, G. (2016). Air pollution in perspective: Health risks of air pollution expressed in equivalent numbers of passively smoked cigarettes. *Environmental Research*, *148*, 475–483. https://doi.org/10.1016/j.envres.2016.04.001

Vassura, I., Venturini, E., Marchetti, S., Piazzalunga, A., Bernardi, E., Fermo, P., & Passarini, F. (2014). Markers and influence of open biomass burning on atmospheric particulate size and composition during a major bonfire event. *Atmospheric Environment*, *82*, 218–225. Retrieved from http://www.sciencedirect.com/science/article/pii/S1352231013007905, https://doi.org/10.1016/j.atmosenv.2013.10.037

Veres, P. R., & Roberts, J. M. (2015). Development of a photochemical source for the production and calibration of acyl peroxynitrate compounds. *Atmospheric Measurement Techniques*, *8*(5), 2225–2231. Retrieved from http://www.atmos-meas-tech.net/8/2225/2015/, https://doi.org/10.5194/amt-8-2225-2015

Veres, P. R., Roberts, J. M., Wild, R. J., Edwards, P. M., Brown, S. S., Bates, T. S., et al. (2015). Peroxynitric acid (HO_2NO_2) measurements during the UBWOS 2013 and 2014 studies using iodide ion chemical ionization mass spectrometry. *Atmospheric Chemistry and Physics*, *15*(14), 8101–8114. Retrieved from http://www.atmos-chem-phys.net/15/8101/2015/, https://doi.org/10.5194/acp-15-8101-2015

Walser, M. L., Desyaterik, Y., Laskin, J., Laskin, A., & Nizkorodov, S. A. (2008). High-resolution mass spectrometric analysis of secondary organic aerosol produced by ozonation of limonene. *Physical Chemistry Chemical Physics*, *10*(7), 1009–1022.

Wood, C. R., Arnold, S. J., Balogun, A. A., Barlow, J. F., Belcher, S. E., Britter, R. E., et al. (2009). Dispersion experiments in central London: The 2007 DAPPLE project. *Bulletin of the American Meteorological Society*, *90*(7), 955–969.

Woodrow, J. E., LePage, J. T., Miller, G. C., & Hebert, V. R. (2014). Determination of methyl isocyanate in outdoor residential air near metam-sodium soil fumigations. *Journal of Agricultural and Food Chemistry*, *62*(36), 8921–8927. https://doi.org/10.1021/jf501696a

Woodward-Massey, R., Taha, Y. M., Moussa, S. G., & Osthoff, H. D. (2014). Comparison of negative-ion proton-transfer with iodide ion chemical ionization mass spectrometry for quantification of isocyanic acid in ambient air. *Atmospheric Environment*, *98*, 693–703. Retrieved from http://www.sciencedirect.com/science/article/pii/S1352231014007079, https://doi.org/10.1016/j.atmosenv.2014.09.014

World Health Organization (2006). WHO Air quality guidelines for particulate matter, ozone, nitrogen dioxide and sulfur dioxide: global update 2005: summary of risk assessment (pp.1–22). Geneva: World Health Organization.

World Health Organization (2015). Residential heating with wood and coal: Health impacts and policy options in Europe and North America. Retrieved from http://ehsdiv.sph.berkeley.edu/krsmith/publications/2015/ResidentialHeatWoodCoal.pdf

Yao, L., Wang, M.-Y., Wang, X.-K., Liu, Y.-J., Chen, H.-F., Zheng, J., et al. (2016). Detection of atmospheric gaseous amines and amides by a high resolution time-of-flight chemical ionization mass spectrometer with protonated ethanol reagent ions. *Atmospheric Chemistry and Physics Discussions*, 1–32. Retrieved from http://www.atmos-chem-phys-discuss.net/acp-2016-484/

Yokelson, R. J., Goode, J. G., Ward, D. E., Susott, R. A., Babbitt, R. E., Wade, D. D., et al. (1999). Emissions of formaldehyde, acetic acid, methanol, and other trace gases from biomass fires in North Carolina measured by airborne Fourier transform infrared spectroscopy. *Journal of Geophysical Research*, *104*(D23), 30,109–30,125. https://doi.org/10.1029/1999JD900817

Yokelson, R. J., Griffith, D. W. T., & Ward, D. E. (1996). Open-path Fourier transform infrared studies of large-scale laboratory biomass fires. *Journal of Geophysical Research*, *101*(D15), 21,067–21,080. https://doi.org/10.1029/96JD01800

Yokelson, R. J., Urbanski, S. P., Atlas, E. L., Toohey, D. W., Alvarado, E. C., Crounse, J. D., et al. (2007). Emissions from forest fires near Mexico City. *Atmospheric Chemistry and Physics*, *7*(21), 5569–5584. https://doi.org/10.5194/acp-7-5569-2007

Yuan, B., Liggio, J., Wentzell, J., Li, S. M., Stark, H., Roberts, J. M., et al. (2015). Secondary formation of nitrated phenols: Insights from observations during the Uintah Basin Winter Ozone Study (UBWOS) 2014. *Atmospheric Chemistry and Physics Discussions*, *15*(20), 28,659–28,697. Retrieved from http://www.atmos-chem-phys-discuss.net/15/28659/2015/, https://doi.org/10.5194/acpd-15-28659-2015